Electronic Supplementary Material (ESI) for Catalysis Science & Technology.

Supporting Information

Increasing Electrochemical Chlorine over Oxygen Selectivity by Optimal Weakening of Oxygen Bonds in Transition Metal-Doped RuO_2

Sulay Saha[1], Koshal Kishor[1,3], and Raj Ganesh S Pala[1,2]

[1]Department of Chemical Engineering, Indian Institute of Technology, Kanpur, 208016, India

[2]Materials Science Programme, Indian Institute of Technology, Kanpur, 208016, India

[3]Institute of Advanced Research, Koba Institutional Area, Gandhinagar, 382426, India

[*]Corresponding authors: rpala@iitk.ac.in

Section 1: Computational Details:

Six valence electrons for each O atom ($2s^2$ $2p^4$) and fourteen valence electrons for each Ru atom ($4p^6 5s^2 4d^6$) are taken into account while performing calculations. The electronic configuration of dopant atoms of Ti, V, Cr, Mn, Fe, Co, Ni, Cu and Zn are given as follows in Table S1:

Table S1: Electronic configuration of elements in the pseudopotential.

Dopants	Electronic Configuration in the used pseudopotential
Ti	$3p63d^3 4s^1$
V	$3p^6 3d^4 4s^1$
Cr	$3p^6 3d^5 4s^1$
Mn	$3p^6 3d^5 4s^2$
Fe	$3d^7 s^1$
Co	$3d^8 4s^1$
Ni	$3p^6 3d^8 4s^2$
Cu	$3d^{10} 4s^1$
Zn	$3d^{10} 4s^2$

The DFT calculations were restricted to 2 × 1 surface unit cells using a 4× 4 Monkhorst Pack *k*-point mesh for slab calculations. A Fermi smearing of 0.1 eV and Pulay mixing is used to ensure the fast convergence of the self-consistent electron density. The energy convergence criterion of 10^{-5} eV was used for structure relaxation. Atomic positions are relaxed until the sum of the absolute forces is less than 0.05 eV/A˚. The DFT + U approach has been used

only for dopants that form strongly correlated oxide systems. The U values of 3.9, 5.0, 3.6, and 6.45 eV for Mn, Fe, Co, and Ni, respectively, were adopted from previous literature reports to better describe the metal d electrons.[1, 2] The 2×1 surface unit cell of the stoichiometric RuO_2 (110) contains two bridge (Ru_{2br}) and two cus sites (Ru_{cus}). We consider adsorption of O_{br}, OH_{br}, OCl_{br}, and Cl_{br} at bridge sites (Ru_{2br}) and adsorption of O_{cus}, OH_{cus}, OCl_{cus}, Cl_{cus}, $(O_2)_{cus}$ and OOH_{cus} at cus sites (Ru_{cus}).

Section 2: CER mechanism:

Three potential reaction mechanisms for the CER are discussed in the literature. The Volmer–Tafel mechanism consists of the adsorption and discharge of two chloride ions (Volmer step) followed by the recombination of two adjacent adsorbed chlorine species and the evolution of Cl_2 (Tafel step)[3, 4]:

$$2(\text{-}O_{br}\text{-}*_{cus})\text{-}O_{ads} + 2\ Cl^- \rightarrow 2(\text{-}O_{br}\text{-}*_{cus})\text{-}(OCl)_{ads} + 2\ e^-$$

$$2(\text{-}O_{br}\text{-}*_{cus})\text{-}(OCl)_{ads} \rightarrow 2(\text{-}O_{br}\text{-}*_{cus})\text{-}O_{ads} + Cl_2$$

The Volmer–Heyrovsky mechanism comprises of the Volmer step, which is followed by the direct recombination of the adsorbed chlorine species with a chloride ion from electrolyte solution accompanied by an electron transfer and the release of Cl_2 (Heyrovsky step)[5]:

$$(\text{-}O_{br}\text{-}*_{cus})\text{-}O_{ads} + Cl^- \rightarrow (\text{-}O_{br}\text{-}*_{cus})\text{-}(OCl)_{ads} + e^-$$

$$(\text{-}O_{br}\text{-}*_{cus})\text{-}(OCl)_{ads} + Cl^- \rightarrow (\text{-}O_{br}\text{-}*_{cus})\text{-}O_{ads} + Cl_2 + e^-$$

The Krishtalik mechanism is quite similar to the Volmer–Heyrovsky mechanism. However, after the Volmer step, a further electron transfer takes place to form an adsorbed chloronium species, which subsequently recombines with a chloride species from the electrolyte solution to form Cl_2.[6]

$$(\text{-}O_{br}\text{-}*_{cus})\text{-}O_{ads} + Cl^- \rightarrow (\text{-}O_{br}\text{-}*_{cus})\text{-}(OCl)_{ads} + e-$$

$$(\text{-}O_{br}\text{-}*_{cus})\text{-}(OCl)_{ads} \rightarrow (\text{-}O_{br}\text{-}*_{cus})\text{-}(OCl)_{ads}^{+} + e-$$

$$(\text{-}O_{br}\text{-}*_{cus})\text{-}(OCl)_{ads}^{+} + Cl^- \rightarrow (\text{-}O_{br}\text{-}*_{cus})\text{-}O_{ads} + Cl_2$$

Among these three reaction mechanisms, the Volmer-Heyrovsky reaction is said to be the most favourable for CER[7, 8].

Section 3: Adsorption energies:

All the adsorption energies were calculated with respect to gaseous Cl_2, gaseous H_2 and H_2O vapor at 298 K and 0.035 bar. The unoccupied Ru_{cus} atoms denoted as ($*_{cus}$) serve as reference with the neighboring *cus* site occupied by O-adsorbate as O- coverage is found on the surface at the concerned electrochemical CER conditions[9]. We obtain the following equations:

$$\Delta E(O*_{cus}) = E(O*_{cus}) - E(*_{cus}) - H_2O + H_2 \cdot$$

$$\Delta E(HO*_{cus}) = E(HO*_{cus}) - E(*_{cus}) - H_2O + \tfrac{1}{2}\cdot H_2$$

$$\Delta E(HOO^*_{cus}) = E(HOO^*_{cus}) - E(^*_{cus}) - H_2O + {}_{3/2}\cdot H_2$$

$$\Delta E(Cl^*_{cus}) = E(Cl^*_{cus}) - E(^*_{cus}) - \tfrac{1}{2}\cdot Cl_2$$

$$\Delta E(ClO^*_{cus}) = E(ClO^*_{cus}) - E(^*_{cus}) - H_2O - \tfrac{1}{2}\cdot Cl_2 + H_2$$

Section 4: Gibbs energies:

The change in free energy change is given by the following reactions

$$\Delta G\,(pH, U) = \Delta E + \Delta E_{ZPE} - T\Delta S$$

The entropy correction is done by following relation[10],

$$S = k_B ln \prod_{i=1}^{N} \frac{1}{1 - \exp(\frac{h\omega_{X,i}}{2\pi k_B T})}$$

Where i is the specific vibrational mode, N is the total number of vibrational modes for reaction intermediate X, k_B is the Boltzmann constant and T is the absolute temperature. All the gases and vapors are assumed to behave ideally and are summarized in Table S2.

Table S2. Zero-point energy (ZPE) and entropies of the water vapor and diatomic gases involved in electrochemical conditions.

Gas	ZPE (eV)	TS (eV)
H_2O (l)	0.57	0.67 (at 0.035 bar)
H_2	0.35	0.40
Cl_2	0.06	0.69

Section 5: pH and electrochemical potential (U) correction:

The relation between free energy change of reaction (ΔG), pH and applied electrochemical potential U is derived using the first principle thermodynamical methodology using reversible hydrogen and reversible chloride electrode as references and as follows:

$$\Delta G\,(pH, U) = \Delta E + \Delta E_{ZPE} - T\Delta S - 0.059\nu(H^+)pH - \nu(e^-)eU - \nu\,(Cl^-)eU_{Cl}$$

Where U_{Cl} is the reversible electrochemical potential for CER in SHE, i.e. 1.36 V.

Two conditions are considered:

Case 1: There is a high concentration of chloride ions, and its concentration is kept constant through the use of supporting electrolytes.

$$\Delta G\,(pH, U) = \Delta E + \Delta E_{ZPE} - T\Delta S - 0.059\nu(H^+)pH - \nu(e^-)eU - \nu\,(Cl^-)eU_{Cl}$$

Case 2: Both the activity of chloride and proton are the same

$$a\,(H^+) = a\,(Cl^-)$$

and the change in free energy is given by the following equation,

$$\Delta G\,(pH, U) = \Delta E + \Delta E_{ZPE} - T\Delta S - 0.059[\nu(H^+) + \nu\,(Cl^-)]pH - \nu(e^-)eU - \nu\,(Cl^-)eU_{Cl}$$

In the present case, the electrochemical reaction is carried out in the acidic medium in presence of a supporting electrolyte which leads to the above equation being reduced into the following form,

$$\Delta G\,(pH = 0.0, U) = \Delta E + \Delta E_{ZPE} - T\Delta S - \nu(e^-)eU - \nu\,(Cl^-)eU_{Cl}$$

Depending upon the adsorbate interaction with the surface, the stoichiometric co-efficient of $\nu(e^-)$ and $\nu\,(Cl^-)$ has been found to vary. The values of $\nu(e^-)$ and $\nu\,(Cl^-)$ upon different adsorbate interaction with the surface leading to different surface structures under reaction conditions are listed below (Table S3),

Table S3. The stoichiometric coefficients $\nu(H^+)$, $\nu(Cl^-)$ and $\nu(e^-)$ for each of the considered adsorbate structures. O_{br} + $*_{cus}$ denotes the reference state.

Surface Structure	$\boldsymbol{\nu(H^+)}$	$\boldsymbol{\nu(e^-)}$	$\boldsymbol{\nu(Cl^-)}$
$\mathbf{O_{br}}$	0	0	0
$\mathbf{O_{br} + Cl_{cus}}$	0	1	-1
$\mathbf{O_{br} + HO_{cus}}$	1	1	0
$\mathbf{O_{br} + O_{cus}}$	2	2	0
$\mathbf{HO_{br} + O_{cus}}$	3	3	0
$\mathbf{O_{br} + HOO_{cus}}$	3	3	0
$\mathbf{O_{br} + ClO_{cus}}$	2	3	-1

Section 6: Accuracy of the calculations:

In the interest of reducing computational demands, most practical DFT calculations are performed using the frozen-core approximation pseudopotential where only the electrons that are important in forming bonds are considered. Among the different numbers of electrons considered while performing the same calculations, some of the examples are given following:

(1) Hansen et al. considered the electrons of 4d and 5s valence shell of Ru at the RPBE level[11]. The usage of a smaller core has led to major changes in the Pourbaix diagram of RuO_2. Also, minor changes in scaling relationship and adsorption energies would occur.

(2) Gropen et al.[12] and Pettersson and Strömberg[13] considered the impact of the exchange interactions between same-shell s-p and d-electrons to achieve higher accuracy[12, 13].

In the case of adsorption of O on RuO_2, it is important to treat not only the valence electrons, but also the electrons in the same shell. While comparing calculations done using different

codes, there are various factors that cause differences in adsorption energy values. However, this should not lead to a difference in the final outcome when compared with the experiment, and the adsorption energy values should be as close to those from values using all-electron codes.

When performing computations, the major factor that causes variation in energy values is the choice of pseudo-potential. In the present calculations, we have used the PBE variation of GGA pseudo-potentials. It has been observed that depending upon the number of electrons considered in pseudopotential while computing, the energy values differ. There are examples of RuO_2 chemisorption studies using PBE that show considerable differences in the adsorption energy when using RPBE[14]. It has been generally accepted that adsorption energies computed using PBE pseudopotential give higher values than those computed using RPBE[14]. Among other reasons that are responsible for the change in adsorption energy values include the number of layers considered while computing and the number of layers allowed to relax. Using a higher number of layers improves accuracy at the cost of higher computational time.

It is well known that GGA pseudo-potentials tend to delocalize electrons due to the self-interaction error[15, 16]. The self-interaction error is an issue for semiconductor materials such as MnO_2 or TiO_2 where lower band-gaps of materials are computed theoretically in comparison to experimental values[17]. Furthermore, for some doped systems, states that have been observed localized experimentally, are found to be delocalized at the GGA level during computation[18]. One of the ways to incorporate the self-interaction error is to implement a Hubbard-U correction on the d-orbitals of transition metals[17]. Rutile TiO_2 is one such example where Hubbard-U-corrections are necessary to describe its electronic properties[18-20], though RuO_2 is well-described without using a U-parameter[21]. On implementing Hubbard-U correction for GGA pseudo-potentials (referred to as GGA+U), fractional occupations of chosen orbitals are disfavoured and constraining electrons to localize in the chosen orbitals[17, 18]. However, there is no general rule for choosing the U value, and the search for the optimal U value is empirical in nature. On top of it, it may happen that different U values are needed to achieve agreement with experimental data for different materials properties of the same material[20]. As for example, García-Mota *et al.* has found that a value of U= 2.1 eV is required to achieve an agreement with the experimental enthalpy of formation of $Ti_2O_3 \rightarrow TiO_2$ while U= 5 eV is required to achieve an agreement with the experimental band-gap on d states of Ti atom in rutile TiO_2[20]. It is to be noted that the choice of U-value depends on which GGA functional is being used[19] and that in general, increasing the U value to obtain the correct band gap is done at the cost of a poorer description of adsorbate-surface bonding[20].

The values of adsorption energies are not affected much due to application of the Hubbard-U parameters. Valdés et al. compared O_{cus} adsorption energies on (110) surface of rutile TiO_2 using both PBE and a self-interaction corrected formulation of the PBE functional and found a difference of only 30 meV[22]. RuO_2 has metallic conductivity[23] and is described well without a U-parameter and the application of a U-value does not lead to an improved description of Ru. For Ti-doped RuO_2, the application of U-values in the range between 1-6 eV on d-orbitals of Ti-atom changes the electronic adsorption energy for O_{cus} by less than 20

meV[24]. Furthermore, Himmetoglu et al.[17] note that application of the GGA+U in the fully localized limit (as implemented in GPAW[18, 25]) can significantly worsen the description of metallic materials. This leads us to conclude that the self-interaction errors appear small enough to ignore in this study.

$$\Delta G\ (pH, U) = \Delta E_{tot} + \Delta E_{ZPE} - T\Delta S - 0.059\, pH.\nu(H^+) - \nu(e^-)eU - \nu(Cl^-)eU_{Cl}$$

$$\Delta G\ (H^+) = 0.5\Delta G_{H2}$$

Section 7: Experimental Details:

Section 7.1: Material Characterization

X-ray powder-diffraction data were collected over the 2θ range 20–70° with Cu-Kα (40 kV, 40 mA) radiation on a Siemens D5000 Bragg-Brentano θ–2θ diffractometer equipped with a diffracted-beam graphite monochromator crystal, 2 mm (1°) divergence and anti-scatter slits, 0.6 mm receiving slit, and incident beam soller slit. The compositions of the electrodes were measured through X-ray fluorescence spectroscopy (ZSX primus series, Rigaku corporation spectrometer). The surface elemental compositions at different depth of the electrodes are analyzed by X-ray Photoelectron Spectroscopy (XPS) using a PHI VersaProbe II Scanning XPS Microprobe with Al K-alpha x-ray source. All XPS results were calibrated by setting the C1s peak to a binding energy of 284.6 eV.

Section 7.2: Electrochemical Characterization

(0.5 M NaCl + 1 M HCl) solution was used to perform all the electrochemical characterizations at room temperature. Pt mesh was used as a counter electrode, and Ag/AgCl (saturated KCl) was used as a reference electrode to measure all potentials reported. Potentiostat (Auto Lab PGSTAT302N) was used to perform linear sweep voltammetry (LSV) and CV of the electrodes in a single-compartment cell. The scan rate for CV measurements was 10 mV/s. The potential window of 0-1.6V (vs Ag/AgCl) was maintained while performing the electrochemical characterizations.

Section 7.3: Gas Measurement Technique

Generated active chlorine species are detected in the reaction solution using a standard colorimetric method approved by USEPA (US Environmental Protection Agency) that uses DPD (N,N-diethyl-p-phenylenediamine) reagent (Hach) and UV-VIS spectrophotometer (Varian Cary 50 Bio).[26] A sample solution (5 mL) is extracted from the electrolyte after performing chronoamperometry with doped and undoped RuO_2 in the range of electrochemical potential of 1.55 – 1.85 V vs RHE for 5 minutes. After that a powder pillow containing DPD reagent is added and shaken thoroughly followed by the appearance of a pink color confirming reaction completion. The absorbance of the pink solution is measured using UV-vis spectrophotometer at 530 nm wavelength against a blank. Using the absorbance values, the unknown concentrations of chlorine are determined.

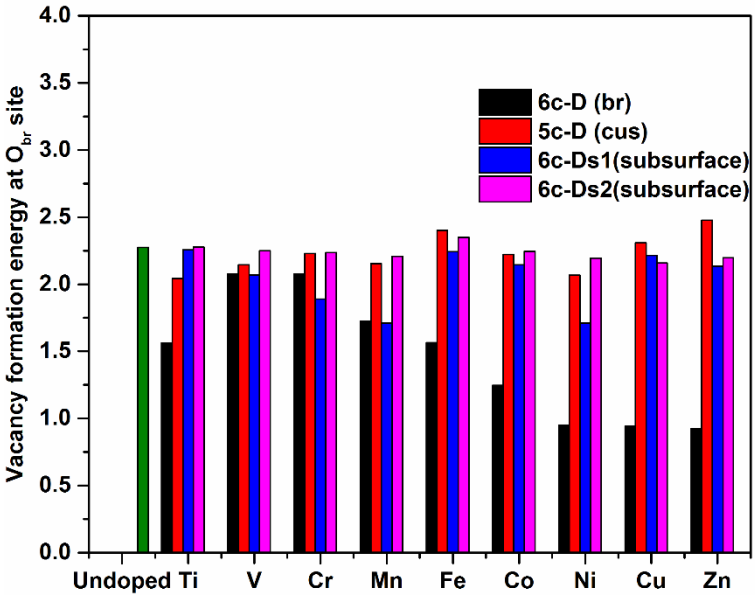

Figure S1: Oxygen vacancy formation energy at bridge site with dopants occupying surface 'cus' site, surface 'br' site and subsurface sites (Ds1 and Ds2).

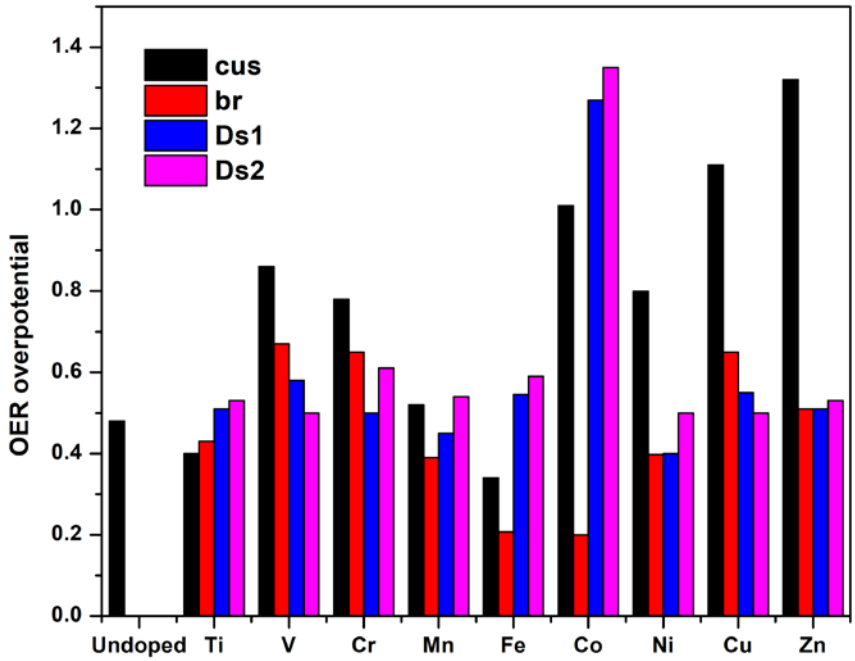

Figure S2: Theoretical overpotential (η^{OER}) of OER on undoped RuO_2 (110) and first-row transition metal-doped RuO_2 (110) surface. The transition-metal is doped at surface 'cus' site, surface 'br' site and subsurface sites (Ds1 and Ds2).

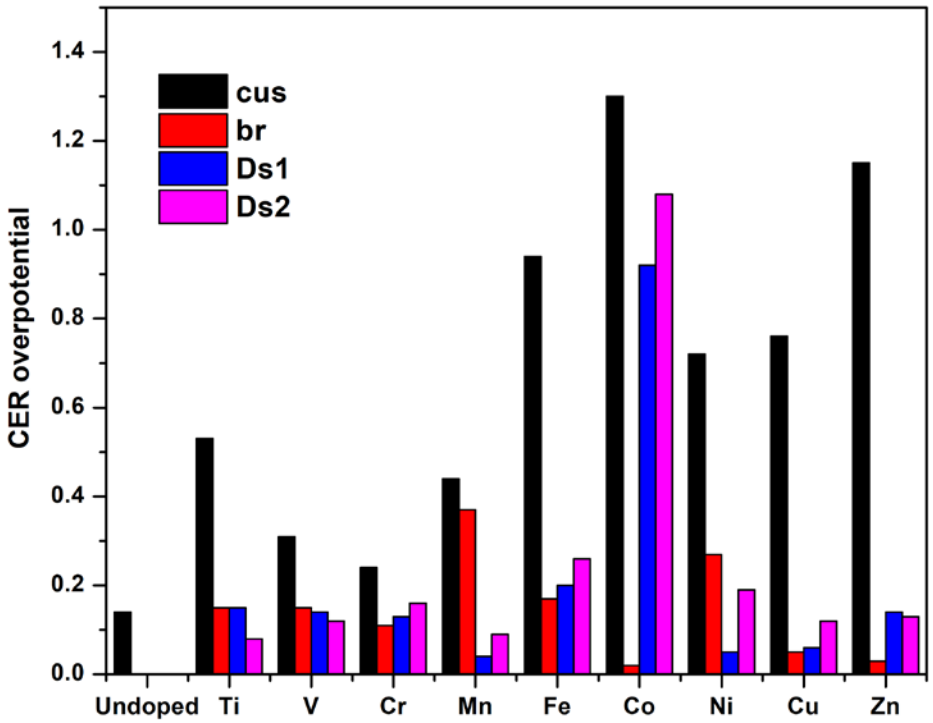

Figure S3: Theoretical overpotential (η^{CER}) of CER on undoped RuO_2 (110) and first-row transition metal-doped RuO_2 (110) surface. The transition-metal is doped at surface 'cus' site, surface 'br' site and subsurface sites (Ds1 and Ds2).

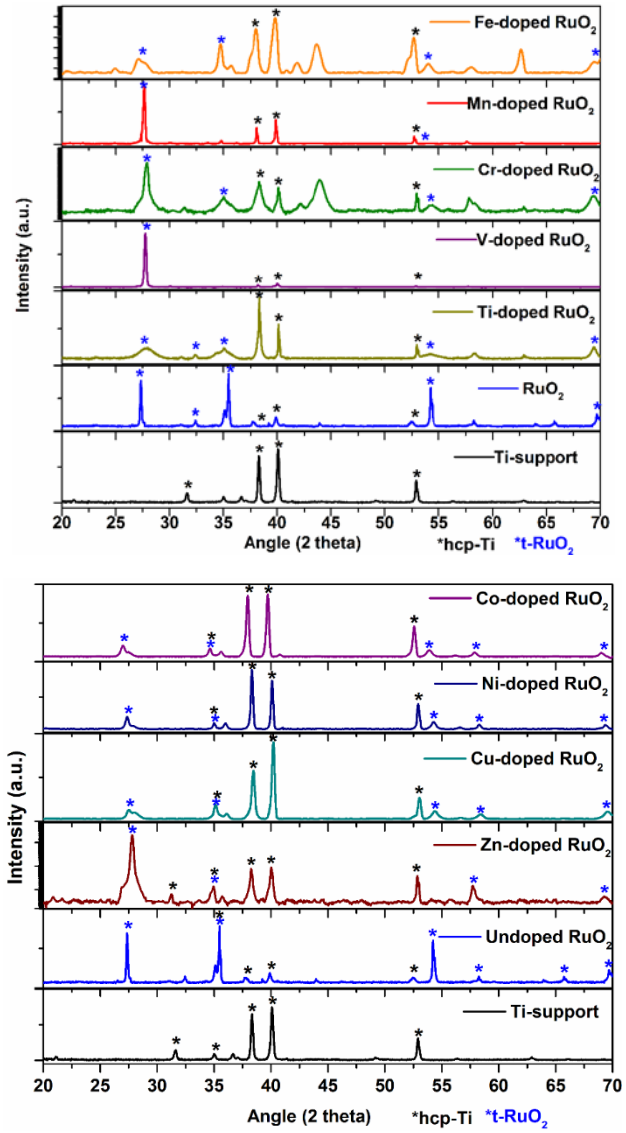

Figure S4: XRD of (Top) Fe-, Mn-, Cr-, V-, Ti, (bottom) Co-, Ni-, Cu-, Zn-doped and undoped RuO_2 on Ti support. These doped samples correspond to the maximum CER selectivity obtained by the respective dopants. The XRD of Ti-support without any electrodeposited layer is also given.

Table S1. Depth profile analysis of ($Ru_{0.98}Zn_{0.02}O_x$) electrodes through XPS.

Depth (nm)	Ru (%)	Zn (%)
0	99.6	<0.4
0-2.5	98.2	1.8
2.5-5	98.5	1.5
5-7.5	98.9	1.1
7.5-10	98.0	2.0

Table S2. Depth profile analysis of ($Ru_{0.98}Cu_{0.02}O_x$) electrodes through XPS.

Depth (nm)	Ru (%)	Cu (%)
0	99.6	<0.4
0-2.5	97.3	2.7
2.5-5	98.4	1.6
5-7.5	98.3	1.7
7.5-10	98.0	2.0

References:

1. L. Wang, T. Maxisch and G. Ceder, *Phys. Rev. B*, 2006, **73**, 195107.
2. S. Liu, Y. Chang, N. He, S. Zhu, L. Wang and X. Liu, *ACS Appl. Mater. Interfac.*, 2023, **15**, 20563-20570.
3. K. S. Exner, J. Anton, T. Jacob and H. Over, *Angew. Chem.*, 2014, **53**, 11032-11035.
4. V. Petrykin, K. Macounova, O. A. Shlyakhtin and P. Krtil, *Angew. Chem.*, 2010, **122**, 4923-4925.
5. L. Janssen, L. Starmans, J. Visser and E. Barendrecht, *Electrochim. Acta*, 1977, **22**, 1093-1100.
6. L. Krishtalik, *Electrochim. Acta*, 1981, **26**, 329-337.
7. K. S. Exner, J. Anton, T. Jacob and H. Over, *Electrocatal.*, 2015, **6**, 163-172.
8. K. S. Exner, J. Anton, T. Jacob and H. Over, *Electrochim. Acta*, 2014, **120**, 460-466.
9. J. Rossmeisl, Z.-W. Qu, H. Zhu, G.-J. Kroes and J. K. Nørskov, *J. Electroanal. Chem.*, 2007, **607**, 83-89.
10. A. Hellman and R. G. Pala, *J. Phys. Chem. C*, 2011, **115**, 12901-12907.
11. H. A. Hansen, I. C. Man, F. Studt, F. Abild-Pedersen, T. Bligaard and J. Rossmeisl, *Phys. Chem. Chem. Phys.*, 2010, **12**, 283-290.
12. O. Gropen, U. Wahlgren and L. Pettersson, *Chem. Phys.*, 1982, **66**, 459-464.
13. A. Strömberg, *Chem. Phys. Lett.*, 1983, **99**, 122-128.
14. F. Abild-Pedersen and M. P. Andersson, *Surf. Sci.*, 2007, **601**, 1747-1753.
15. J. P. Perdew and A. Zunger, *Phys. Rev. B*, 1981, **23**, 5048.
16. J. P. Perdew, A. Ruzsinszky, J. Tao, V. N. Staroverov, G. E. Scuseria and G. I. Csonka, *J. Chem. Phys.*, 2005, **123**, 062201.
17. B. Himmetoglu, A. Floris, S. Gironcoli and M. Cococcioni, *Int. J. Quantum Chem.*, 2014, **114**, 14-49.
18. J. Stausholm-Mo-ller, H. H. Kristoffersen, B. Hinnemann, G. K. Madsen and B. Hammer, *J. Chem. Phys.*, 2010, **133**, 144708.
19. B. J. Morgan and G. W. Watson, *J. Phys. Chem. C*, 2009, **113**, 7322-7328.
20. M. n. García-Mota, A. Vojvodic, F. Abild-Pedersen and J. K. Nørskov, *J. Phys. Chem. C*, 2012, **117**, 460-465.
21. H. Over, *Chem. Rev.*, 2012, **112**, 3356-3426.
22. A. Valdes, J. Brillet, M. Grätzel, H. Gudmundsdottir, H. A. Hansen, H. Jonsson, P. Klüpfel, G.-J. Kroes, F. Le Formal and I. C. Man, *Phys. Chem. Chem. Phys.*, 2012, **14**, 49-70.
23. W. Dmowski, T. Egami, K. E. Swider-Lyons, C. T. Love and D. R. Rolison, *J. Phys. Chem. B*, 2002, **106**, 12677-12683.
24. R. K. Karlsson, H. A. Hansen, T. Bligaard, A. Cornell and L. G. Pettersson, *Electrochim. Acta*, 2014, **146**, 733-740.
25. S. Dudarev, G. Botton, S. Savrasov, C. Humphreys and A. Sutton, *Phys. Rev. B*, 1998, **57**, 1505.
26. P. Gayen, S. Saha and V. Ramani, *ACS Appl. Energy Mater.*, 2020, **3**, 3978-3983.